Simulation Methodology for Inference on Physical Parameters of Complex Vector-Valued Signals

S. Chandna and A. T. Walden, *Senior Member, IEEE*

Swati Chandna and Andrew Walden are both at the Department of Mathematics, Imperial College London, 180 Queen's Gate, London SW7 2BZ, UK. (e-mail: s.chandna09@imperial.ac.uk and a.walden@imperial.ac.uk)

Abstract

Complex-valued vector time series occur in diverse fields such as oceanography and meteorology, and scientifically interpretable parameters may be estimated from them. We show that it is possible to make inference such as confidence intervals on these parameters using a vector-valued circulant embedding simulation method, combined with bootstrapping. We apply the methodology to three parameters of interest in oceanography, and compare the resulting simulated confidence intervals with those computed using analytic results. We conclude that the simulation scheme offers an inference approach either in the absence of theoretical distributional results, or to check the effect of nuisance parameters where theoretical results are available.

Keywords

Bootstrapping vector-valued time series; circulant embedding; coherence; complex-valued signals; ellipse orientation; rotary coefficient

I. Introduction

Vector time series such as current and wind are typically resolved into orthogonal components which may be represented as the real and imaginary parts of a complex-valued time series. For motion taking place in a plane, geometrical information is encoded in these structures; this is quite different from taking two arbitrary real-valued series and combining them to form a complex-valued series when there is no reason to consider the data to be generated by motion in the complex plane.

In this paper we develop simulation methodology which enables inference to be drawn on parameters derived from such complex-valued vector time series. (The methodology can also be used for real-valued vector time series.) By choosing some parameters for which theoretical inferential results are known, we are able to validate our simulation methodology.

The parameters we have chosen arise in the rotary analysis method [10], [11], [13], [19] which decomposes motions on the complex plane into counter-rotating components which have proved particulary useful in the study of geophysical flows influenced by the rotation of the Earth. For example, inertial waves in oceanography have clockwise/counterclockwise polarization in the northern/southern hemisphere, and since the spectrum of the complex-valued time series is asymmetric about zero frequency it is possible to readily distinguish between clockwise and counterclockwise effects — e.g. see [27].

For the simulation, computationally efficient multivariate circulant embedding is used to generate portions of realizations whose spectral density function (SDF) matrix is given by the estimated SDF matrix derived from the observed series. Percival and Constantine [20] showed that it is always possible to use exact circulant embedding for simulating a real-valued *scalar* time series from a Gaussian stationary process given an SDF estimate produced by a suitable non-negative nonparametric estimator. The resulting simulated time series will have statistical properties closely resembling those of the process under study. For vector-valued processes we show, using cross-spectrum estimators of bilinear form, how a *multivariate* circulant embedding approach can likewise be developed. Our circulant embedding approach correctly treats the covariance structure for the practical situation of finite samples. Combined with parametric bootstrapping, estimated confidence intervals for the parameters are forthcoming, and may be compared to those derived theoretically.

The main use of the simulation methodology would be expected to be for parameters for which theoretical results are unavailable; however it is also useful to test the theoretical results when plug-in estimates of nuisance parameters are needed, as is the case for the first and third parameters examined here.

The paper is organized as follows. Section II covers basic structures and notation for complex-valued p-vector-valued time series. Then we discuss ocean current data, the parameters of interest, their estimation, theoretical confidence intervals, and an analysis of the assumption of Gaussianity in Section III. In Section IV we briefly review circulant matrices, leading to a description of the circulant embedding algorithm for vector-valued circulant embedding based on [5]. In Section V we formulate our method for exact multivariate circulant embedding for simulating a time series given a suitable SDF estimate. Section VI looks at bootstrap confidence intervals for parameters. Results are presented in Section VII, and concluding remarks are provided in Section VIII.

II. Structures and Notation

We consider a *p-vector-valued discrete time stochastic process* $\{\boldsymbol{Z}_t\}$ whose tth element, $t \in \mathbb{Z}$, is the column vector $\boldsymbol{Z}_t = [Z_{1,t}, \ldots, Z_{p,t}]^T \in \mathbb{C}^p$, and without loss of generality assume each component process has zero mean. We assume the p processes are *jointly* second-order stationary (SOS): with * denoting complex-conjugation, the cross-covariance sequence and cross-relation sequence are respectively, $\mathrm{cov}\{Z_{l,t+\tau}, Z_{m,t}\} \equiv E\{Z_{l,t+\tau} Z^*_{m,t}\}$ and $\mathrm{rel}\{Z_{l,t+\tau}, Z_{m,t}\} \equiv$

$E\{Z_{l,t+\tau}Z_{m,t}\}$, $1 \le l,m \le p$, $\tau \in \mathbb{Z}$, and are functions of τ only [22]. With ^{T} and ^{H} denoting transpose and conjugate-transpose, the matrix-valued autocovariance sequence (ACVS) is then $\boldsymbol{s}_{\boldsymbol{Z},\tau} = \mathrm{cov}\{\boldsymbol{Z}_{t+\tau}, \boldsymbol{Z}_t\} = E\{\boldsymbol{Z}_{t+\tau}\boldsymbol{Z}_t^H\}$, where we define $s_{\boldsymbol{Z},lm,\tau} \equiv (\boldsymbol{s}_{\boldsymbol{Z},\tau})_{lm}$, and the matrix-valued relation sequence is then $\boldsymbol{r}_{\boldsymbol{Z},\tau} = \mathrm{rel}\{\boldsymbol{Z}_{t+\tau}, \boldsymbol{Z}_t^T\} = E\{\boldsymbol{Z}_{t+\tau}\boldsymbol{Z}_t^T\}$, with $r_{\boldsymbol{Z},lm,\tau} \equiv (\boldsymbol{r}_{\boldsymbol{Z},\tau})_{lm}$. From their definitions we see that $s_{\boldsymbol{Z},lm,\tau} = s^*_{\boldsymbol{Z},ml,-\tau}$ and $r_{\boldsymbol{Z},lm,\tau} = r_{\boldsymbol{Z},ml,-\tau}$, $\quad 1 \le l,m \le p$. We assume that, $\sum_{\tau=-\infty}^{\infty} |s_{\boldsymbol{Z},lm,\tau}| < \infty$ and $\sum_{\tau=-\infty}^{\infty} |r_{\boldsymbol{Z},lm,\tau}| < \infty$, for $1 \le l \le m \le p$, which means that the corresponding Fourier transforms, $S_{\boldsymbol{Z},lm}(f)$ and $R_{\boldsymbol{Z},lm}(f)$, for $1 \le l,m \le p$, exist and are bounded and continuous. We now append the conjugate vector-valued process to obtain [7], [22], [24]

$$\boldsymbol{U}_t = [Z_{1,t}, \ldots, Z_{p,t}, Z^*_{1,t}, \ldots, Z^*_{p,t}]^T = [\boldsymbol{Z}_t^T, \boldsymbol{Z}_t^H]^T, \tag{1}$$

with $\boldsymbol{U}_t \in \mathbb{C}^{2p}$, for which

$$\boldsymbol{s}_{\boldsymbol{U},\tau} \equiv E\{\boldsymbol{U}_{t+\tau}\boldsymbol{U}_t^H\} = \begin{bmatrix} \boldsymbol{s}_{\boldsymbol{Z},\tau} & \boldsymbol{r}_{\boldsymbol{Z},\tau} \\ \boldsymbol{r}^*_{\boldsymbol{Z},\tau} & \boldsymbol{s}^*_{\boldsymbol{Z},\tau} \end{bmatrix}.$$

The corresponding spectral matrix is given by

$$\boldsymbol{S}_{\boldsymbol{U}}(f) = \Delta_{\mathrm{t}} \sum_{\tau=-\infty}^{\infty} \boldsymbol{s}_{\boldsymbol{U},\tau} \mathrm{e}^{-\mathrm{i}2\pi f \tau \Delta_{\mathrm{t}}} = \begin{bmatrix} \boldsymbol{S}_{\boldsymbol{Z}}(f) & \boldsymbol{R}_{\boldsymbol{Z}}(f) \\ \boldsymbol{R}^*_{\boldsymbol{Z}}(-f) & \boldsymbol{S}^*_{\boldsymbol{Z}}(-f) \end{bmatrix},$$

where $S_{\boldsymbol{Z},lm}(f) = [\boldsymbol{S}_{\boldsymbol{Z}}(f)]_{lm}, R_{\boldsymbol{Z},lm}(f) = [\boldsymbol{R}_{\boldsymbol{Z}}(f)]_{lm}$ and Δ_{t} is the sample interval.

Now write $Z_{l,t} = X_{l,t} + \mathrm{i}Y_{l,t}$, with $X_{l,t} = \mathrm{Re}\{Z_{l,t}\}$ and $Y_{l,t} = \mathrm{Im}\{Z_{l,t}\}$, (where $\mathrm{Re}\{\cdot\}$ and $\mathrm{Im}\{\cdot\}$ refer to real and imaginary parts), for $l = 1, \ldots, p$, and define the real-valued vector-valued process $\boldsymbol{V}_t \in \mathbb{R}^{2p}$, as

$$\boldsymbol{V}_t = [X_{1,t}, \ldots, X_{p,t}, Y_{1,t}, \ldots, Y_{p,t}]^T = [\boldsymbol{X}_t^T, \boldsymbol{Y}_t{}^T]^T. \tag{2}$$

Denoting the $p \times p$ identity matrix by $\boldsymbol{I}_p$ we have

$$\boldsymbol{U}_t = \boldsymbol{T}_p \boldsymbol{V}_t, \tag{3}$$

with

$$\boldsymbol{T}_p = \begin{bmatrix} \boldsymbol{I}_p & \mathrm{i}\boldsymbol{I}_p \\ \boldsymbol{I}_p & -\mathrm{i}\boldsymbol{I}_p \end{bmatrix}, \tag{4}$$

and $\boldsymbol{s}_{\boldsymbol{U},\tau} = \boldsymbol{T}_p \boldsymbol{s}_{\boldsymbol{V},\tau} \boldsymbol{T}_p^H \Rightarrow \boldsymbol{S}_{\boldsymbol{U}}(f) = \boldsymbol{T}_p \boldsymbol{S}_{\boldsymbol{V}}(f) \boldsymbol{T}_p^H$, where

$$\boldsymbol{s}_{\boldsymbol{V},\tau} \equiv E\{\boldsymbol{V}_{t+\tau}\boldsymbol{V}_t^T\} = \begin{bmatrix} \boldsymbol{s}_{\boldsymbol{X}\boldsymbol{X},\tau} & \boldsymbol{s}_{\boldsymbol{X}\boldsymbol{Y},\tau} \\ \boldsymbol{s}_{\boldsymbol{Y}\boldsymbol{X},\tau} & \boldsymbol{s}_{\boldsymbol{Y}\boldsymbol{Y},\tau} \end{bmatrix}. \tag{5}$$

The corresponding spectral matrix is given by

$$\boldsymbol{S_V}(f) = \Delta_{\mathrm{t}} \sum_{\tau=-\infty}^{\infty} \boldsymbol{s}_{\boldsymbol{V},\tau} \mathrm{e}^{-\mathrm{i}2\pi f \tau \Delta_{\mathrm{t}}} = \begin{bmatrix} \boldsymbol{S_{XX}}(f) & \boldsymbol{S_{XY}}(f) \\ \boldsymbol{S_{YX}}(f) & \boldsymbol{S_{YY}}(f) \end{bmatrix}.$$

Likewise, $\boldsymbol{V}_t = \boldsymbol{A}_p \boldsymbol{U}_t$, with

$$\boldsymbol{A}_p = \tfrac{1}{2} \begin{bmatrix} \boldsymbol{I}_p & \boldsymbol{I}_p \\ -\mathrm{i}\boldsymbol{I}_p & \mathrm{i}\boldsymbol{I}_p \end{bmatrix}, \tag{6}$$

and $\boldsymbol{s}_{\boldsymbol{V},\tau} = \boldsymbol{A}_p \boldsymbol{s}_{\boldsymbol{U},\tau} \boldsymbol{A}_p^H \Rightarrow \boldsymbol{S_V}(f) = \boldsymbol{A}_p \boldsymbol{S_U}(f) \boldsymbol{A}_p^H$. Thus the problem of efficiently simulating from a p-variate complex-valued process $\{\boldsymbol{Z}_t\}$ is reduced to the problem of efficiently simulating from the corresponding $2p$-variate real-valued process $\{\boldsymbol{V}_t\}$ with known second-order statistics, followed by the transformation to $\{\boldsymbol{U}_t\}$ via (3), and the extraction of $\{\boldsymbol{Z}_t\}$ from $\{\boldsymbol{U}_t\}$.

We note that

$$\boldsymbol{S_Z}(\pm f) = \boldsymbol{S_{XX}}(f) + \boldsymbol{S_{YY}}(f) \pm 2\mathrm{Im}\{\boldsymbol{S_{XY}}(f)\} \tag{7}$$

$$\boldsymbol{R_Z}(f) = \boldsymbol{S_{XX}}(f) - \boldsymbol{S_{YY}}(f) + \mathrm{i}2\mathrm{Re}\{\boldsymbol{S_{XY}}(f)\}, \tag{8}$$

III. Ocean Current Parameters and Estimators

A. The Data

The data we consider consists of ocean current time series at six depths (110, 760, 1260, 1760, 2510, and 3476 m) in the Labrador Sea [16], [17]. The measurement of current speed in the eastward and northward direction at any of these depths are associated with, respectively, the real component $\{X_t\}$, and the imaginary component $\{Y_t\}$, of $\{Z_t\}$. Interest is concentrated in low frequencies around the inertial frequency of about 0.07 cycles per hour (c/h). Since we have 6 scalar complex-valued time series we identify them as $\{Z_{1.t}\}, \ldots, \{Z_{6,t}\}$ if necessary; if one of these is understood we just use $\{Z_t\}$.

B. The Parameters

The first parameter is derived for single complex-valued time series, the second for pairs of time series, and the third for single time series but with the complication that the quantity is angular.

Since $\{Z_t\}$ is SOS with zero mean it has the spectral representation given by $Z_t = \int_{-f_{\mathcal{N}}}^{f_{\mathcal{N}}} \mathrm{e}^{\mathrm{i}2\pi f t\, \Delta_{\mathrm{t}}}\, \mathrm{d}Z(f)$, $t \in$

$\mathbb{Z}$, where $Z(f)$ is an orthogonal process. At frequency magnitude $|f|$ the contribution to $\{Z_t\}$ is

$$\begin{aligned} Z_t(f) &= |\mathrm{d}Z(f)|\mathrm{e}^{\mathrm{i}\arg\{\mathrm{d}Z(f)\}}\mathrm{e}^{\mathrm{i}2\pi f t\Delta_\mathrm{t}} \\ &+ |\mathrm{d}Z(-f)|\mathrm{e}^{\mathrm{i}\arg\{\mathrm{d}Z(-f)\}}\mathrm{e}^{-\mathrm{i}2\pi f t\Delta_\mathrm{t}}, \end{aligned} \tag{9}$$

the parametric equation of a *random* ellipse, comprising the addition of two oppositely rotating motions (rotary components) with random amplitudes and phases.

The first parameter we consider is the *rotary coefficient* [11] for any one of the single complex-valued processes, so $p = 1$. This coefficient satisfies $-1 \leq \rho(f) \leq 1$ and measures the tendency of a complex-valued process to rotate in a counterclockwise or clockwise manner at frequency f; it provides an objective means of quantifying the rotation associated with the asymmetry of the spectrum of the complex-valued process $\{Z_t\}$ [24, p. 210]. Let $f > 0$. It is defined as

$$\rho(f) = [S_Z(f) - S_Z(-f)]/[S_Z(f) + S_Z(-f)], \tag{10}$$

where $S_Z(f)\mathrm{d}f = E\{|\mathrm{d}Z(f)|^2\}$ and $S_Z(-f)\mathrm{d}f = E\{|\mathrm{d}Z(-f)|^2\}$. It has been extensively applied — see [6] for details. Then if $\rho(f) = +1$, (i.e., $S_Z(-f) = 0$), then motion is all counterclockwise circular at that frequency, whereas if $\rho(f) = -1$, (i.e., $S_Z(f) = 0$), then motion is all clockwise circular at that frequency, and if $\rho(f) = 0$, then there is rectilinear motion (unidirectional flow). Using (7) we see that $\rho(f)$ can also be written as $\rho(f) = [2\mathrm{Im}\{S_{XY}(f)\}]/[S_{XX}(f) + S_{YY}(f)]$, but this is not so easily interpretable as (10).

The second parameter we shall consider is called the *outer coherence* for any two of the complex-valued processes, $\{Z_{l,t}\}$ and $\{Z_{m,t}\}$ say, measured simultaneously at two different spatial locations [11, p. 496], [19]. So here $p = 2$. It is defined as

$$\gamma^2_{lm*}(f) = [|R_{\boldsymbol{Z},lm}(f)|^2]/[S_{\boldsymbol{Z},ll}(f)S_{\boldsymbol{Z},mm}(-f)], \tag{11}$$

and is the magnitude-squared coherence between $\{Z_{l,t}\}$ and the complex-conjugate of $\{Z_{m,t}\}$. It is interpreted in [11], [19] as measuring the coherence between counter-rotating components. Using (7) and (8) this can be rewritten in terms of the real processes by noting that

$$\begin{aligned} |R_{\boldsymbol{Z},lm}(f)|^2 &= [S_{XX,lm}(f) - S_{YY,lm}(f)]^2 + 4\mathrm{Re}^2\{S_{XY,lm}(f)\} \\ S_{\boldsymbol{Z},ll}(\pm f) &= S_{XX,ll}(f) - S_{YY,ll}(f) \pm 2\mathrm{Im}\{S_{XY,ll}(f)\}. \end{aligned}$$

The final parameter is the *mean orientation* of the elliptical motion of any of the single complex-valued processes. The orientation or azimuth is the angle which the major axis of the ellipse

(9) makes with the horizontal (x-direction). Since the ellipses are random, there will be a mean orientation, long of interest to oceanographers [11],[13] and this is given by [23]

$$\theta(f) = \tfrac{1}{2}\arg\{R_{\boldsymbol{Z}}(f)\}. \tag{12}$$

This can be rewritten in terms of the spectra of the real processes in the form

$$\theta(f) = \tfrac{1}{2}\arctan\left\{[2\mathrm{Im}\{S_{XY}(f)\}]/[S_{XX}(f) - S_{YY}(f)]\right\}$$

where $\arctan\{\cdot\}$ is the "four quadrant inverse tangent" and $-\pi/2 \leq \theta < \pi/2$.

We now turn our attention to estimating these parameters which requires spectral matrix estimation.

C. Spectral Matrix Estimation via Multitapering

The spectral matrix estimation method used here is as follows. We start with a set of K real-valued orthonormal tapers $\{h_{k,t}, t = 0, \ldots, N-1\}$, for $k = 0, \ldots, K-1$. Form the product $\{h_{k,t}\boldsymbol{U}_t, \}$ of the kth taper with $\{\boldsymbol{U}_t, t = 0, \ldots, N-1\}$, and then compute its Fourier transform

$$\boldsymbol{J}_{\boldsymbol{U},k}(f) = \Delta_{\mathrm{t}}^{1/2} \sum_{t=0}^{N-1} h_{k,t} \begin{bmatrix} \boldsymbol{Z}_t \\ \boldsymbol{Z}_t^* \end{bmatrix} \mathrm{e}^{-\mathrm{i}2\pi f t\,\Delta_{\mathrm{t}}} = \begin{bmatrix} \boldsymbol{J}_{\boldsymbol{Z},k}(f) \\ \boldsymbol{J}_{\boldsymbol{Z},k}^*(-f) \end{bmatrix},$$

where $\boldsymbol{J}_{\boldsymbol{Z},k}(f) \equiv \Delta_{\mathrm{t}}^{1/2} \sum_{t=0}^{N-1} h_{k,t}\boldsymbol{Z}_t \mathrm{e}^{-\mathrm{i}2\pi \mathrm{f} t\,\Delta_{\mathrm{t}}}$. To estimate $\boldsymbol{S}_{\boldsymbol{U}}(f)$ we average over the spectral estimates formed from the different taperings:

$$\hat{\boldsymbol{S}}_{\boldsymbol{U}}(f) = \frac{1}{K}\sum_{k=0}^{K-1} \boldsymbol{J}_{\boldsymbol{U},k}(f)\boldsymbol{J}_{\boldsymbol{U},k}^H(f) = \begin{bmatrix} \hat{\boldsymbol{S}}_{\boldsymbol{Z}}(f) & \hat{\boldsymbol{R}}_{\boldsymbol{Z}}(f) \\ \hat{\boldsymbol{R}}_{\boldsymbol{Z}}^*(-f) & \hat{\boldsymbol{S}}_{\boldsymbol{Z}}^*(-f) \end{bmatrix}. \tag{13}$$

(Many details on multitapering in the scalar case are given in [21]). Now $\boldsymbol{U}_t = \boldsymbol{T}_p\boldsymbol{V}_t$, so we can also write

$$\begin{aligned} \boldsymbol{J}_{\boldsymbol{U},k}(f) &= \boldsymbol{T}_p\Delta_{\mathrm{t}}^{1/2} \sum_{t=0}^{N-1} h_{k,t} \begin{bmatrix} \boldsymbol{X}_t \\ \boldsymbol{Y}_t \end{bmatrix} \mathrm{e}^{-\mathrm{i}2\pi f t\,\Delta_{\mathrm{t}}} \\ &\equiv \boldsymbol{T}_p \begin{bmatrix} \boldsymbol{J}_{\boldsymbol{X},k}(f) \\ \boldsymbol{J}_{\boldsymbol{Y},k}(f) \end{bmatrix} \equiv \boldsymbol{T}_p\boldsymbol{J}_{\boldsymbol{V},k}(f), \end{aligned}$$

so that an alternative form for the spectral matrix estimator is

$$\hat{\boldsymbol{S}}_{\boldsymbol{U}}(f) = \frac{1}{K}\sum_{k=0}^{K-1} \boldsymbol{T}_p\boldsymbol{J}_{\boldsymbol{V},k}(f)\boldsymbol{J}_{\boldsymbol{V},k}^H(f)\boldsymbol{T}_p^H = \boldsymbol{T}_p\hat{\boldsymbol{S}}_{\boldsymbol{V}}(f)\boldsymbol{T}_p^H,$$

where

$$\hat{\boldsymbol{S}}_{\boldsymbol{V}}(f) = \begin{bmatrix} \hat{\boldsymbol{S}}_{\boldsymbol{XX}}(f) & \hat{\boldsymbol{S}}_{\boldsymbol{XY}}(f) \\ \hat{\boldsymbol{S}}_{\boldsymbol{YX}}(f) & \hat{\boldsymbol{S}}_{\boldsymbol{YY}}(f) \end{bmatrix}.$$

Under Gaussianity, $\{\boldsymbol{J}_{\boldsymbol{V},k}(f), k = 0, \ldots, K-1\}$ are distributed independently and identically with a complex Gaussian distribution with mean $\boldsymbol{0}$ and covariance matrix $\boldsymbol{S}_{\boldsymbol{V}}(f)$, (e.g., [6]) written as

$$\boldsymbol{J}_{\boldsymbol{V},k}(f) \sim \mathcal{N}_2^C(\boldsymbol{0}, \boldsymbol{S}_{\boldsymbol{V}}(f)), \quad W_N \le |f| \le f_{\mathcal{N}} - W_N. \tag{14}$$

Here $2W_N$ is the width of the spectral window induced by tapering. For sine tapers $W_N = (K+1)/[2(N+1)\Delta_{\mathrm{t}}]$, (e.g., [28]), which decreases to zero as $N \to \infty$ for a fixed K. Also, the frequency band within which the overall spectral window due to tapering [28] is concentrated, must be narrow enough that the components of $\boldsymbol{S}_{\boldsymbol{V}}(f)$ are essentially constant across it. Likewise, since $\boldsymbol{J}_{\boldsymbol{U},k}(f) = \boldsymbol{T}\boldsymbol{J}_{\boldsymbol{V},k}(f)$, and $\boldsymbol{S}_{\boldsymbol{U}}(f) = \boldsymbol{T}\boldsymbol{S}_{\boldsymbol{V},k}(f)\boldsymbol{T}^H$,

$$\boldsymbol{J}_{\boldsymbol{U},k}(f) \sim \mathcal{N}_2^C(\boldsymbol{0}, \boldsymbol{S}_{\boldsymbol{U}}(f)), \quad W_N \le |f| \le f_{\mathcal{N}} - W_N. \tag{15}$$

Finally, $K\hat{\boldsymbol{S}}_{\boldsymbol{V}}(f) = \sum_{k=0}^{K-1} \boldsymbol{J}_{\boldsymbol{V},k}(f)\boldsymbol{J}_{\boldsymbol{V},k}^H(f)$ and $K\hat{\boldsymbol{S}}_{\boldsymbol{U}}(f) = \sum_{k=0}^{K-1} \boldsymbol{J}_{\boldsymbol{U},k}(f)\boldsymbol{J}_{\boldsymbol{U},k}^H(f)$, and so provided $K \ge 2$, (to avoid matrix singularity), under Gaussianity the distribution of $K\hat{\boldsymbol{S}}_{\boldsymbol{V}}(f)$ is 2-D complex Wishart with K complex degrees of freedom and mean $K\boldsymbol{S}_{\boldsymbol{V}}(f)$, [14] which we denote by

$$K\hat{\boldsymbol{S}}_{\boldsymbol{V}}(f) \sim \mathcal{W}_2^C\{K, \boldsymbol{S}_{\boldsymbol{V}}(f)\}, \; W_N \le |f| \le f_{\mathcal{N}} - W_N. \tag{16}$$

Similarly,

$$K\hat{\boldsymbol{S}}_{\boldsymbol{U}}(f) \sim \mathcal{W}_2^C\{K, \boldsymbol{S}_{\boldsymbol{U}}(f)\}, \; W_N \le |f| \le f_{\mathcal{N}} - W_N. \tag{17}$$

D. Theoretical Confidence Intervals for Parameters

The first parameter $\rho(f)$ involves any single series, $\{Z_t\}$ say. With $\boldsymbol{U}_t = [Z_t, Z_t^*]^T$ the estimator $\hat{\rho}(f)$ follows by replacing $S_Z(\pm f)$ in (10) by the diagonal entries of the 2×2 matrix $\hat{\boldsymbol{S}}_{\boldsymbol{U}}(f)$ as given in (13). Under the assumption that the process $\{\boldsymbol{V}_t\}$ is a stationary Gaussian process, the theoretical distribution of the estimator follows from (15) or (17); see [6] for details on the derivation of the theoretical confidence interval for $\rho(f)$. The distribution of $\hat{\rho}(f)$ and a confidence interval for $\rho(f)$ both depend on

$$\gamma_*^2(f) = |R_Z(f)|^2/[S_Z(f)S_Z(-f)], \tag{18}$$

the (magnitude-squared) coherence between $\{Z_t\}$ and its complex-conjugate $\{Z_t^*\}$. In practice this coherence can be estimated and debiased to give $\bar{\gamma}_*^2(f)$, and plugged into the formula for the confidence interval. The resulting confidence interval can then be compared to that derived later from the simulation scheme to verify the efficacy of the plug-in estimate $\bar{\gamma}_*^2(f)$.

Now consider the second parameter $\gamma_{lm*}^2(f)$ which involves series l and m. Take $\boldsymbol{U}_t = [Z_{l,t}, Z_{m,t}, Z_{l,t}^*, Z_{m,t}^*]^T$. The estimator $\hat{\gamma}_{lm*}^2(f)$ follows by use of the appropriate entries of the 4×4 matrix $\hat{\boldsymbol{S}}_{\boldsymbol{U}}(f)$ as given in (13). Under the assumption that the process $\{\boldsymbol{V}_t\}$ is a stationary Gaussian process, the theoretical distribution of the estimator follows from (15) or (17) and theoretical confidence intervals for the outer coherence (11) can be found using [29]. Unlike for the rotary coefficient, in this case there is no nuisance parameter. Note that for the lth series, $\gamma_*(f) \equiv \gamma_{ll*}(f)$.

For the mean orientation estimator $\hat{\theta}(f) = \frac{1}{2}\arg\{\hat{R}_Z(f)\}$, the derivation of confidence intervals uses circular distributions and is given in Appendix-A and involves the replacement of a median by a mean and use of the plug-in estimate $\bar{\gamma}_*^2(f)$. A comparison of such a confidence interval with the simulated one can be used to discern any effect of the median/mean replacement and the use of the plug-in estimate.

E. Gaussianity

Later we will compare the just-formulated theoretical confidence intervals to those simulated using the circulant embedding/resampling methodology soon to be discussed. The theoretical confidence intervals assume that the process $\{\boldsymbol{V}_t\}$ is a Gaussian process, i.e., all of its finite dimensional distributions are multivariate Gaussian [2, p. 36]. As we will see, the simulation also produces vector-valued time series realizations with elements which are multivariate Gaussian. It is critical therefore that such an assumption is not obviously contradicted by the data.

Consider the ocean current data at each depth. Rather than just examine the marginal distributions of the X_t and Y_t components for Gaussianity, we look instead at the vector $[X_t, Y_t]^T$; Gaussianity of this bivariate quantity is a necessary, but not sufficient condition for Gaussianity of $\{\boldsymbol{V}_t\}$, but of course in reality we cannot examine all finite dimensional distributions. This at least could provide some supporting evidence that the assumption of being a sample from a Gaussian process is reasonable, and therefore that the proposed comparison of the confidence intervals makes sense.

We use the idea of bivariate Q-Q (quantile-quantile) plots and implement some of the ideas discussed in [18]. Some details of the construction of the plots is given in Appendix-B. Using

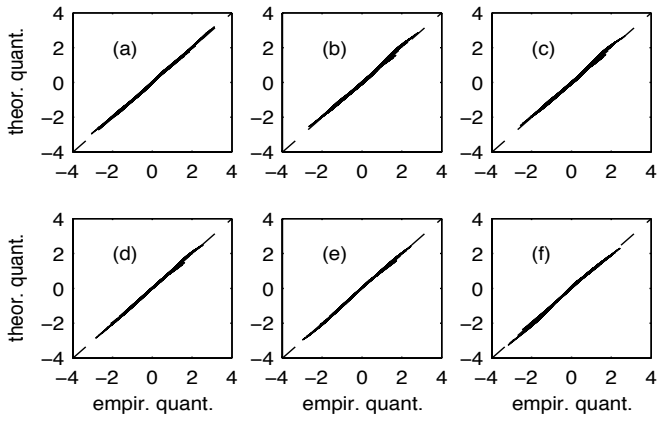

Fig. 1. Q-Q plots for standardized eastward ocean current speeds, $\{\check{V}_{i1}\}$, the empirical quantiles, against theoretical spherical Gaussian quantiles at depths (m): (a) 110, (b) 760, (c) 1260, (d) 1760, (e) 2510, and (f) 3476. The dashed diagonal line is the ideal 45^o line.

$\{\boldsymbol{V}_i = [X_i, Y_i]^T, i = 1, \ldots, 1600\}$, for each of the recording depths, six pairs of such Q-Q plots were calculated. Denoting the normalized vector by $\check{\boldsymbol{V}}_i = [\check{V}_{i1}, \check{V}_{i2}]^T$, (see Appendix-B), Fig. 1 shows the bivariate Q-Q plots for eastward measurements. (Results for northward measurements were very similar and are not shown.) The linearity of these Q-Q plots implies behaviour consistent with what would be expected from a Gaussian process, and do not contradict our Gaussianity assumption.

IV. Vector-Valued Circulant Embedding

We now consider the use of the circulant embedding technique to simulate realizations from $\{\boldsymbol{V}_t\}$ as this method is exact and computationally fast.

A. Circulant Matrices

The $m \times m$ circulant matrix for the sequence $c = \{c_0, \ldots, c_{m-1}\}$ is

$$\boldsymbol{C}_m = \text{circ}\{c\} = \begin{bmatrix} c_0 & c_1 & c_2 & \ldots & c_{m-1} \\ c_{m-1} & c_0 & c_1 & \ldots & c_{m-2} \\ \vdots & \vdots & \vdots & \ldots & \vdots \\ c_1 & c_2 & c_3 & \ldots & c_0 \end{bmatrix}.$$

Then $\boldsymbol{C}_m = \boldsymbol{F}_m \boldsymbol{\Lambda}_m \boldsymbol{F}_m^H$, where $\boldsymbol{\Lambda}_m = \text{diag}\{\lambda_0, \ldots, \lambda_{m-1}\}$ is a diagonal matrix of eigenvalues of $\boldsymbol{C}_m$ and each eigenvalue λ_k of $\boldsymbol{C}_m$ is given by the discrete Fourier transform (DFT) of the

elements of c, i.e., $\lambda_k = \sum_{j=0}^{m-1} c_j \mathrm{e}^{-\mathrm{i}2\pi jk/m}$ for $k = 0, \ldots, m-1$. $\boldsymbol{F}_m$ is an $m \times m$ unitary matrix with (j,k)th element given by $(\boldsymbol{F}_m)_{jk} = m^{-1/2}\mathrm{e}^{-\mathrm{i}2\pi jk/m}$ for $0 \le j,k \le m-1$. A proof for this result is given in [3, p.134].

B. Key Ideas

We wish to generate at least one length-N realization $\boldsymbol{\mathcal{V}} = [\boldsymbol{V}_0^T, \ldots, \boldsymbol{V}_{N-1}^T]^T$ with $\boldsymbol{V}_t$ defined by (2) with *a priori* specified ACVS, $\{\boldsymbol{s}_{\boldsymbol{V},\tau}\}$, (a sequence of $2p \times 2p$ matrices). For example, if $p = 1$ then $\boldsymbol{\mathcal{V}} = [[X_{1,0}, Y_{1,0}], \ldots, [X_{1,N-1}, Y_{1,N-1}]]^T$. Once the $\boldsymbol{V}_0, \ldots, \boldsymbol{V}_{N-1}$, are known, (3) can be used to produce the $\boldsymbol{U}_0, \ldots, \boldsymbol{U}_{N-1}$, with $\boldsymbol{U}_t$ containing the required $Z_{1,t}, \ldots, Z_{p,t}$.

Our approach is based on [5]. Let $\boldsymbol{\Sigma}_{\boldsymbol{\mathcal{V}}} \equiv E\{\boldsymbol{\mathcal{V}}\boldsymbol{\mathcal{V}}^T\}$. The matrix autocovariance sequence for $\{\boldsymbol{V}_t\}$ is defined as $\boldsymbol{s}_{\boldsymbol{V},\tau} = E\{\boldsymbol{V}_{t+\tau}\boldsymbol{V}_t^T\}$, so that, for example, $\boldsymbol{s}_{\boldsymbol{V},\tau} = \boldsymbol{s}_{\boldsymbol{V},-\tau}^T$. It then follows that $\boldsymbol{\Sigma}_{\boldsymbol{\mathcal{V}}}$ is a block Toeplitz matrix ($2pN \times 2pN$) given by

$$\boldsymbol{\Sigma}_{\boldsymbol{\mathcal{V}}} = \begin{bmatrix} \boldsymbol{s}_{\boldsymbol{V},0} & \boldsymbol{s}_{\boldsymbol{V},1}^T & \boldsymbol{s}_{\boldsymbol{V},2}^T & \cdots & \boldsymbol{s}_{\boldsymbol{V},N-1}^T \\ \boldsymbol{s}_{\boldsymbol{V},1} & \boldsymbol{s}_{\boldsymbol{V},0} & \boldsymbol{s}_{\boldsymbol{V},1}^T & \cdots & \boldsymbol{s}_{\boldsymbol{V},N-2}^T \\ \vdots & \vdots & \vdots & \ddots & \vdots \\ \boldsymbol{s}_{\boldsymbol{V},N-1} & \boldsymbol{s}_{\boldsymbol{V},N-2} & \boldsymbol{s}_{\boldsymbol{V},N-3} & \cdots & \boldsymbol{s}_{\boldsymbol{V},0} \end{bmatrix}$$

The strategy is to embed the block Toeplitz matrix, $\boldsymbol{\Sigma}_{\boldsymbol{\mathcal{V}}}$, in a larger block circulant matrix, say $\boldsymbol{\Sigma}_{\tilde{\boldsymbol{\mathcal{V}}}}$, and then simulate a vector, say $\tilde{\boldsymbol{\mathcal{V}}}$, having this covariance matrix. Define the block circulant matrix $\boldsymbol{\Sigma}_{\tilde{\boldsymbol{\mathcal{V}}}} = \mathrm{circ}\{\boldsymbol{c}\}, \boldsymbol{c} = \{\boldsymbol{c}_0, \ldots, \boldsymbol{c}_{m_1-1}\}$, with

$$\boldsymbol{c}_j = \begin{cases} \boldsymbol{s}_{\boldsymbol{V},j}^T & 0 \le j \le \lfloor m_1/2 \rfloor; \\ \boldsymbol{s}_{\boldsymbol{V},m_1-j} & \lfloor m_1/2 \rfloor < j \le m_1 - 1; \end{cases} \tag{19}$$

with the recommendation in [5] to take $m_1 \ge 2N-2$.

For $\boldsymbol{\Sigma}_{\tilde{\boldsymbol{\mathcal{V}}}}$ to be a valid covariance matrix it must be symmetric and non-negative definite (NND). Consider the case $N = 3$. As $m_1 \ge 2N-2$, we start with the 'minimal embedding,' i.e., we choose $m_1 = 2N-2 = 4$. Then $\boldsymbol{\Sigma}_{\tilde{\boldsymbol{\mathcal{V}}}}$ is a $2pm_1 \times 2pm_1$ block circulant matrix of the form:

$$\boldsymbol{\Sigma}_{\tilde{\boldsymbol{\mathcal{V}}}} = \begin{bmatrix} \boldsymbol{s}_{\boldsymbol{V},0} & \boldsymbol{s}_{\boldsymbol{V},1}^T & \boldsymbol{s}_{\boldsymbol{V},2}^T & \boldsymbol{s}_{\boldsymbol{V},1} \\ \boldsymbol{s}_{\boldsymbol{V},1} & \boldsymbol{s}_{\boldsymbol{V},0} & \boldsymbol{s}_{\boldsymbol{V},1}^T & \boldsymbol{s}_{\boldsymbol{V},2}^T \\ \boldsymbol{s}_{\boldsymbol{V},2}^T & \boldsymbol{s}_{\boldsymbol{V},1} & \boldsymbol{s}_{\boldsymbol{V},0} & \boldsymbol{s}_{\boldsymbol{V},1}^T \\ \boldsymbol{s}_{\boldsymbol{V},1}^T & \boldsymbol{s}_{\boldsymbol{V},2}^T & \boldsymbol{s}_{\boldsymbol{V},1} & \boldsymbol{s}_{\boldsymbol{V},0} \end{bmatrix}.$$

From the properties of partitioned matrices we know that for $\mathbf{\Sigma}_{\tilde{\boldsymbol{\mathcal{V}}}}$ to be symmetric, i.e., $\mathbf{\Sigma}_{\tilde{\boldsymbol{\mathcal{V}}}} = \mathbf{\Sigma}_{\tilde{\boldsymbol{\mathcal{V}}}}^T$, we will need that $\boldsymbol{s}_{\boldsymbol{V},2}$ be symmetric [1, (eqn. (2.8.1)]. If $\boldsymbol{s}_{\boldsymbol{V},2}$ is not symmetric, then $\mathbf{\Sigma}_{\tilde{\boldsymbol{\mathcal{V}}}}$ is not symmetric. If instead we take $m_1 = 5$, then

$$\mathbf{\Sigma}_{\tilde{\boldsymbol{\mathcal{V}}}} = \begin{bmatrix} \boldsymbol{s}_{\boldsymbol{V},0} & \boldsymbol{s}_{\boldsymbol{V},1}^T & \boldsymbol{s}_{\boldsymbol{V},2}^T & \boldsymbol{s}_{\boldsymbol{V},2} & \boldsymbol{s}_{\boldsymbol{V},1} \\ \boldsymbol{s}_{\boldsymbol{V},1} & \boldsymbol{s}_{\boldsymbol{V},0} & \boldsymbol{s}_{\boldsymbol{V},1}^T & \boldsymbol{s}_{\boldsymbol{V},2}^T & \boldsymbol{s}_{\boldsymbol{V},2} \\ \boldsymbol{s}_{\boldsymbol{V},2} & \boldsymbol{s}_{\boldsymbol{V},1} & \boldsymbol{s}_{\boldsymbol{V},0} & \boldsymbol{s}_{\boldsymbol{V},1}^T & \boldsymbol{s}_{\boldsymbol{V},2}^T \\ \boldsymbol{s}_{\boldsymbol{V},2}^T & \boldsymbol{s}_{\boldsymbol{V},2} & \boldsymbol{s}_{\boldsymbol{V},1} & \boldsymbol{s}_{\boldsymbol{V},0} & \boldsymbol{s}_{\boldsymbol{V},1}^T \\ \boldsymbol{s}_{\boldsymbol{V},1}^T & \boldsymbol{s}_{\boldsymbol{V},2}^T & \boldsymbol{s}_{\boldsymbol{V},2} & \boldsymbol{s}_{\boldsymbol{V},1} & \boldsymbol{s}_{\boldsymbol{V},0} \end{bmatrix},$$

which is symmetric irrespective of the $\boldsymbol{s}_{\boldsymbol{V},\tau}$'s. In general we can only take m_1 to be even if $\boldsymbol{s}_{\boldsymbol{V},m_1/2}$ is symmetric, and if it isn't we must choose m_1 to be odd. In view of the resultant high likelihood of needing to choose m_1 odd, we recommend

$$m_1 > 2N - 2. \tag{20}$$

Now as $\mathbf{\Sigma}_{\tilde{\boldsymbol{\mathcal{V}}}}$ is a $2pm_1 \times 2pm_1$ block circulant matrix, it follows [5] that

$$\mathbf{\Sigma}_{\tilde{\boldsymbol{\mathcal{V}}}} = (\boldsymbol{F}_{m_1} \otimes \boldsymbol{I}_{2p}) \operatorname{diag}\{\boldsymbol{\lambda}_0, \ldots, \boldsymbol{\lambda}_{m_1-1}\} (\boldsymbol{F}_{m_1} \otimes \boldsymbol{I}_{2p})^H, \tag{21}$$

where $\boldsymbol{\lambda}_k$ is the $2p \times 2p$ matrix

$$\boldsymbol{\lambda}_k = \sum_{j=0}^{m_1-1} \boldsymbol{c}_j \, \mathrm{e}^{-\mathrm{i}2\pi jk/m_1}, \qquad k = 0, \ldots, m_1 - 1. \tag{22}$$

When m_1 is odd, $\boldsymbol{c}_j = \boldsymbol{c}_{m_1-j}^T$ for $j = 1, \ldots, m_1 - 1$. When m_1 is even, $\boldsymbol{c}_j = \boldsymbol{c}_{m_1-j}^T$ for $j = 1, \ldots, m_1 - 1$, $j \neq m_1/2$, and $\boldsymbol{s}_{\boldsymbol{V},m_1/2}$ is symmetric. We also know that $w_k^{-j} = w_k^{m_1-j}$ when $w_k \equiv \exp(\mathrm{i}2\pi k/m_1)$. It readily follows that $\boldsymbol{\lambda}_k^H = \boldsymbol{\lambda}_k$, i.e., $\boldsymbol{\lambda}_k$ is Hermitian for each k and has the eigenvalue decomposition [24, p. 270]

$$\boldsymbol{\lambda}_k = \boldsymbol{U}_k \boldsymbol{D}_k \boldsymbol{U}_k^H, \qquad k = 0, \ldots, m_1 - 1. \tag{23}$$

$\boldsymbol{U}_k$ is a $2p \times 2p$ unitary matrix with columns the eigenvectors of $\boldsymbol{\lambda}_k$, and $\boldsymbol{D}_k = \operatorname{diag}\{D_{1,k}, \ldots, D_{2p,k}\}$ is a real diagonal matrix of eigenvalues of $\boldsymbol{\lambda}_k$. Now [1, p. 43]

$$\begin{aligned} &(\operatorname{diag}\{\boldsymbol{U}_0 \boldsymbol{D}_0^{1/2}, \ldots, \boldsymbol{U}_{m_1-1} \boldsymbol{D}_{m_1-1}^{1/2}\})^H \\ &\qquad = \operatorname{diag}\{\boldsymbol{D}_0^{1/2} \boldsymbol{U}_0^H, \ldots, \boldsymbol{D}_{m_1-1}^{1/2} \boldsymbol{U}_{m_1-1}^H\}. \end{aligned}$$

Then $\tilde{\boldsymbol{\mathcal{V}}} \equiv (\boldsymbol{F}_{m_1} \otimes \boldsymbol{I}_{2p}) \operatorname{diag}\{\boldsymbol{U}_0 \boldsymbol{D}_0^{1/2}, \ldots, \boldsymbol{U}_{m_1-1} \boldsymbol{D}_{m_1-1}^{1/2}\} \mathcal{Z}'$, with $\mathcal{Z}' = [\mathcal{Z}_0, \ldots, \mathcal{Z}_{2pm_1-1}]^T$ a vector of independent $\mathcal{N}(0,1)$ variables, gives $\tilde{\boldsymbol{\mathcal{V}}} \sim \mathcal{N}_{2pm_1}(\boldsymbol{0}, \boldsymbol{\Sigma}_{\tilde{\boldsymbol{\mathcal{V}}}})$.

A slight adjustment increases simulation efficiency. Let $\mathcal{Z} = \mathcal{Z}^{(1)} + \mathrm{i}\mathcal{Z}^{(2)}$ where, independently, $\mathcal{Z}^{(\alpha)} \sim \mathcal{N}_{2pm_1}(\boldsymbol{0}, \boldsymbol{I}_{2pm_1}); \alpha = 1, 2$ and set

$$\tilde{\boldsymbol{\mathcal{V}}}' \equiv (\boldsymbol{F}_{m_1} \otimes \boldsymbol{I}_{2p}) \operatorname{diag}\{\boldsymbol{U}_0 \boldsymbol{D}_0^{1/2}, \ldots, \boldsymbol{U}_{m_1-1} \boldsymbol{D}_{m_1-1}^{1/2}\} \mathcal{Z}.$$

Proposition 1: The real and imaginary parts of $\tilde{\boldsymbol{\mathcal{V}}}'$ are vectors having covariance $\boldsymbol{\Sigma}_{\tilde{\boldsymbol{\mathcal{V}}}}$, and are independent of each other.

Proof: $E\{\mathcal{Z}\mathcal{Z}^T\} = \boldsymbol{0}$, while $E\{\mathcal{Z}\mathcal{Z}^H\} = 2\boldsymbol{I}_{2pm_1}$, so that $E\{\tilde{\boldsymbol{\mathcal{V}}}'[\tilde{\boldsymbol{\mathcal{V}}}']^T\} = \boldsymbol{0}$ and $E\{\tilde{\boldsymbol{\mathcal{V}}}'[\tilde{\boldsymbol{\mathcal{V}}}']^H\} = 2\boldsymbol{\Sigma}_{\tilde{\boldsymbol{\mathcal{V}}}}$. Then

$$E\{\mathrm{Re}\{\tilde{\boldsymbol{\mathcal{V}}}'\}[\mathrm{Re}\{\tilde{\boldsymbol{\mathcal{V}}}'\}]^T\} = E\{\mathrm{Im}\{\tilde{\boldsymbol{\mathcal{V}}}'\}[\mathrm{Im}\{\tilde{\boldsymbol{\mathcal{V}}}'\}]^T\} = \boldsymbol{\Sigma}_{\tilde{\boldsymbol{\mathcal{V}}}} \tag{24}$$

$$E\{\mathrm{Re}\{\tilde{\boldsymbol{\mathcal{V}}}'\}[\mathrm{Im}\{\tilde{\boldsymbol{\mathcal{V}}}'\}]^T\} = E\{\mathrm{Im}\{\tilde{\boldsymbol{\mathcal{V}}}'\}[\mathrm{Re}\{\tilde{\boldsymbol{\mathcal{V}}}'\}]^T\} = \boldsymbol{0}. \tag{25}$$

From (24) the real and imaginary parts of $\tilde{\boldsymbol{\mathcal{V}}}'$ are vectors having the required covariance, while from (25) these are uncorrelated, and independent under Gaussianity. ■

C. Choice of m_1.

Since the second step in the algorithm involves computing the discrete Fourier transform of each block $\boldsymbol{c}_j, j = 0, \ldots, m_1 - 1$, we wish m_1 to be as highly composite as possible so as to maximise the efficiency of the FFT algorithm.

Suppose we initially choose $m_1 = 2^g$ for some g such that $m_1 \geq 2N - 2$. Since m_1 is even we need to check that $\boldsymbol{s}_{\boldsymbol{V},m_1/2}$ is symmetric, and if it isn't we can choose $m_1 = 3^g$ for some g for which $m_1 > 2N - 2$. In either case we need to check that $\boldsymbol{\Sigma}_{\tilde{\boldsymbol{\mathcal{V}}}}$ is NND. By (21), $\boldsymbol{\Sigma}_{\tilde{\boldsymbol{\mathcal{V}}}}$ and $\operatorname{diag}\{\boldsymbol{\lambda}_0, \ldots, \boldsymbol{\lambda}_{m_1-1}\}$ are congruent, so $\boldsymbol{\Sigma}_{\tilde{\boldsymbol{\mathcal{V}}}}$ is NND iff $\boldsymbol{\lambda}_k$ is NND for $k = 0, \ldots, m_1 - 1$. To check that $\boldsymbol{\Sigma}_{\tilde{\boldsymbol{\mathcal{V}}}}$ is NND for a particular value of m_1, we need merely to check that the entries of $\operatorname{diag}\{D_{1,k}, \ldots, D_{2p,k}\}$ are non-negative for each k.

In practice, the following algorithm may be used to generate realizations of the vector-valued complex process.

D. Algorithm

1. Choose a suitable $m_1 > 2N - 2$.

2. Find the sequence of $2p \times 2p$ matrices $\{\boldsymbol{\lambda}_k\}$ for $k = 0, 1, \ldots m_1 - 1$ as given by (22) using a FFT algorithm.

3. For $k = 0, 1, \ldots m_1 - 1$, determine $\boldsymbol{U}_k$ and $\boldsymbol{D}_k$ in (23) and simulate two real $2p$-vector-valued independent standard normal vectors $\mathcal{Z}_k^{(\alpha)} \sim \mathcal{N}_{2p}(\boldsymbol{0}, \boldsymbol{I}_{2p}); \alpha = 1, 2$ and set $\boldsymbol{B}_k = \boldsymbol{U}_k \boldsymbol{D}_k^{1/2}(\mathcal{Z}_k^{(1)} + \mathrm{i}\mathcal{Z}_k^{(2)})$.

4. Compute $\tilde{\boldsymbol{V}}'_j = m_1^{-1/2} \sum_{k=0}^{m_1-1} \boldsymbol{B}_k \, \mathrm{e}^{-\mathrm{i}2\pi kj/m_1}, \quad j = 0, \ldots, m_1 - 1$ via an FFT. For each j, $\tilde{\boldsymbol{V}}'_j$ is a complex $2p$-length column vector. $\mathrm{Re}\{\tilde{\boldsymbol{V}}'_\ell\}, \ell = 0, \ldots, N-1$, and $\mathrm{Im}\{\tilde{\boldsymbol{V}}'_\ell\}, \ell = 0, \ldots, N-1$ are two independent realizations.

5. For the complex-valued realizations take $\boldsymbol{U}_\ell = \boldsymbol{T}_p \mathrm{Re}\{\tilde{\boldsymbol{V}}'_\ell\}$, $\ell = 0, \ldots, N-1$. The top p values of $\boldsymbol{U}_\ell$ form a realization of $[Z_{1,\ell}, \ldots, Z_{p,\ell}]^T$. An additional independent realization follows by utilising the imaginary values $\boldsymbol{T}_p \mathrm{Im}\{\tilde{\boldsymbol{V}}'_\ell\}$.

As seen in Section V, in our application the entries of $\mathrm{diag}\,\{D_{1,k}, \ldots, D_{2p,k}\}$ are guaranteed non-negative.

V. Generating multivariate time series using nonparametric spectral estimates

In Section IV we have described simulation methods to generate exact realizations from a perfectly-specified complex vector-valued Gaussian stationary process.

While this is useful for pure simulation purposes, our focus is different. As is commonly the case we have available a single realization of a complex-valued p-vector-valued process, estimate parameters of interest, and we want to make inference on the true parameter values. For real-valued scalar time series Percival and Constantine [20] considered generating portions of realizations whose spectral density function (SDF) is given by an estimated SDF derived from the observed series, thus producing simulated time series whose statistical properties closely resemble the time series under study. They showed that it is always possible to use *exact* circulant embedding for simulating a scalar time series from a scalar Gaussian stationary process given a suitable SDF estimate.

They also compared the use of circulant embedding for bootstrapping time series with other frequency domain methods: the use of DFT phase randomization [25] and DFT phase randomization combined with amplitude modification [8, Chapter 8]. Due to their derivation directly from the DFT, these methods have a problematic circularity assumption built into their realizations, as nicely illustrated in [20]. Circulant embedding does not suffer from this problem.

We study the multivariate case. Once we have an algorithm for generating such real multi-

variate time series, we can either generate complex-valued multivariate time series by applying transformation (3) and work with the simpler complex-valued statistics to get the parameter estimator of interest — and hence its properties via bootstrapping — or formulate the parameter estimators in terms of the more complicated statistics of the real-valued components.

A. NND Properties of Estimated Spectral Matrices

By renaming random variables write $\{\boldsymbol{V}_t\}$ in (2) as $\boldsymbol{V}_t = [V_{1,t}, \ldots, V_{2p,t}]^T$. Let $\hat{\mathbf{S}}_{\boldsymbol{V}}(f)$ denote an estimate of the SDF matrix corresponding to $\{\boldsymbol{V}_t\}$ of the form

$$\hat{\boldsymbol{S}}_{\boldsymbol{V}}(f) = \Delta_{\mathrm{t}} \sum_{\tau=-(N-1)}^{N-1} \hat{\boldsymbol{s}}_{\boldsymbol{V},\tau} \mathrm{e}^{-\mathrm{i}2\pi f \tau \Delta_{\mathrm{t}}}. \tag{26}$$

Here $\{\hat{\boldsymbol{s}}_{\boldsymbol{V},\tau}\}$ is an estimate of the ACVS $\{\boldsymbol{s}_{\boldsymbol{V},\tau}\}$ such that $\hat{\boldsymbol{s}}_{\boldsymbol{V},\tau} = \hat{\boldsymbol{s}}_{\boldsymbol{V},-\tau}^T$ and $\hat{\boldsymbol{s}}_{\boldsymbol{V},\tau} = \mathbf{0}$, $|\tau| \geq N$. $\hat{\mathbf{S}}_{\boldsymbol{V}}(f)$ is a $2p \times 2p$ matrix:

$$\hat{\mathbf{S}}_{\boldsymbol{V}}(f) = \begin{bmatrix} \hat{S}_{\boldsymbol{V},11}(f) & \cdots & \hat{S}_{\boldsymbol{V},1(2p)}(f) \\ \vdots & \ddots & \vdots \\ \hat{S}_{\boldsymbol{V},(2p)1}(f) & \cdots & \hat{S}_{\boldsymbol{V},(2p)(2p)}(f) \end{bmatrix}, \tag{27}$$

with $\hat{\boldsymbol{S}}_{\boldsymbol{V},qr}(f)$ estimating the cross-spectrum between the qth and rth terms of $\{\boldsymbol{V}_t\}$.

The *true* spectral matrix $\boldsymbol{S}(f)$ is NND (e.g., [2, p. 233]). Consider spectral matrix estimators constructed as follows [26]. Define the complex demodulate of the qth process, $q = 1, \ldots, 2p$, by $\omega_{q,t} \equiv V_{q,t} \exp(\mathrm{i}2\pi f t \Delta_{\mathrm{t}})$, a shifting of all the frequency components of $\{V_{q,t}\}$ by f. The process $\{\omega_{q,t}\}$ is also a zero mean stationary process. For any two processes $\{V_{q,t}\}$ and $\{V_{r,t}\}$ consider bilinear form cross-spectral estimators $\hat{S}_{\boldsymbol{V},qr}(f) = \Delta_{\mathrm{t}} \sum_{s=0}^{N-1} \sum_{t=0}^{N-1} V_{q,s} \Phi_{s,t} V_{r,t} \, \mathrm{e}^{\mathrm{i}2\pi f(t-s)\Delta_{\mathrm{t}}} = \Delta_{\mathrm{t}} \boldsymbol{\Omega}_q^H \boldsymbol{\Phi} \boldsymbol{\Omega}_r$, where $\boldsymbol{\Omega}_q$ is $[\omega_{q,0}, \ldots, \omega_{q,N-1}]^T$, and the weight matrix $\boldsymbol{\Phi} \in \mathbb{R}^{N \times N}$ is symmetric, not a function of frequency, does not depend on $\{\omega_{q,t}\}$ and $\{\omega_{r,t}\}$, and is NND in order that $\hat{S}_{\boldsymbol{V},ll}(f) \geq 0$.

Proposition 2: The matrix estimator, $\hat{\boldsymbol{S}}_{\boldsymbol{V}}(f)$, is NND.

Proof: For $p = 1$, $\hat{\boldsymbol{S}}_{\boldsymbol{V}}(f) = \Delta_{\mathrm{t}} \boldsymbol{\Omega} \boldsymbol{\Phi}_2 \boldsymbol{\Omega}^H$, where

$$\boldsymbol{\Omega} = \begin{bmatrix} \boldsymbol{\Omega}_1^H & \mathbf{0} \\ \mathbf{0} & \boldsymbol{\Omega}_2^H \end{bmatrix} \quad \text{and} \quad \boldsymbol{\Phi}_2 = \begin{bmatrix} \boldsymbol{\Phi} & \boldsymbol{\Phi} \\ \boldsymbol{\Phi} & \boldsymbol{\Phi} \end{bmatrix},$$

i.e., $\boldsymbol{\Phi}_2$ is the 2×2 block matrix of $\boldsymbol{\Phi}$'s. But if $\boldsymbol{\Phi}$ is NND, so is $\boldsymbol{\Phi}_2$ [1, p. 301], and $\hat{\boldsymbol{S}}_{\boldsymbol{V}}(f)$ and $\boldsymbol{\Phi}_2$ are congruent, so $\hat{\boldsymbol{S}}_{\boldsymbol{V}}(f)$ is NND. When $p = 2$ we replace $\boldsymbol{\Phi}_2$ by $\boldsymbol{\Phi}_4$, the 4×4 block matrix of

$\boldsymbol{\Phi}$'s, (which is also NND by iteration), and replace $\boldsymbol{\Omega}$ by the block matrix with diagonal entries $\boldsymbol{\Omega}_1^H, \ldots, \boldsymbol{\Omega}_4^H$; then $\hat{\boldsymbol{S}}_{\boldsymbol{V}}(f)$ is again NND, and so on. ■

Estimators which can be written in the specified bilinear form include multitaper estimators, WOSA (Welch's overlapped segment averaging) estimators, and Parzen or Papoulis lag window estimators; see [26] for details. It is assumed hereafter that $\hat{\boldsymbol{S}}_{\boldsymbol{V}}(f)$ is NND. Advantageously, all such bilinear estimators can be rewritten as an average of K direct cross-spectrum estimators (K = rank of $\boldsymbol{\Phi}$), i.e.,

$$\begin{aligned}\hat{S}_{\boldsymbol{V},qr}(f) &= \frac{\Delta_{\mathrm{t}}}{K}\sum_{k=0}^{K-1}\gamma_k\left[\sum_{s=0}^{N-1}h_{k,s}V_{q,s}\mathrm{e}^{-\mathrm{i}2\pi fs\Delta_{\mathrm{t}}}\right]\\ &\times \left[\sum_{t=0}^{N-1}h_{k,t}V_{r,t}\mathrm{e}^{\mathrm{i}2\pi ft\Delta_{\mathrm{t}}}\right],\end{aligned}$$

where the γ_k's are positive weights. Such an estimator is an example of (26) since it can be written as $\hat{S}_{\boldsymbol{V},qr}(f) = \Delta_{\mathrm{t}}\sum_{\tau=-(N-1)}^{N-1}\hat{s}^{(bil)}_{\boldsymbol{V},qr,\tau}\mathrm{e}^{-\mathrm{i}2\pi f\tau\Delta_{\mathrm{t}}}$, where $\hat{s}^{(bil)}_{\boldsymbol{V},qr,\tau}$ is $\sum_{t=0}^{N-\tau-1}h_{k,t+\tau}V_{q,t+\tau}h_{k,t}V_{r,t}$ for $0 \le \tau \le N-1$, and $\sum_{t=-\tau}^{N-1}h_{k,t+\tau}V_{q,t+\tau}h_{k,t}V_{r,t}$ for $-1 \le \tau \le -(N-1)$, and zero otherwise. Note $\hat{\boldsymbol{s}}^{(bil)}_{\boldsymbol{V},\tau} = (\hat{\boldsymbol{s}}^{(bil)}_{\boldsymbol{V},-\tau})^T$. Returning to the form of $\boldsymbol{V}_t$ in (2) we know from [7, p. 2972] that the equivalent spectrum estimator for $\boldsymbol{U}_t$ in (1) follows simply from

$$\hat{\boldsymbol{S}}_{\boldsymbol{U}}(f) = \boldsymbol{T}_p\hat{\boldsymbol{S}}_{\boldsymbol{V}}(f)\boldsymbol{T}_p^H, \tag{28}$$

and then $\hat{\boldsymbol{S}}_{\boldsymbol{Z}}(f)$ is the top-left $p \times p$ submatrix of $\hat{\boldsymbol{S}}_{\boldsymbol{U}}(f)$. The bilinear form we choose to use here is the standard multitaper estimator as described in Section III-C.

B. Generating Multivariate Time Series

$\hat{\mathbf{S}}_{\boldsymbol{V}}(f)$ is the true spectrum for some vector-valued Gaussian stationary process, say $\{\hat{\boldsymbol{V}}_t\}$ (e.g., [30, p. 24]). We wish to generate realizations from $\{\hat{\boldsymbol{V}}_t\}$, using a vector-valued circulant embedding method. In [20] spectral estimates were related to the eigenvalues of the univariate circulant embedding matrix based on the fact that the ACVS of any real-valued scalar process is symmetric. However, the ACVS of a vector-valued process need not be symmetric.

Replacing $\boldsymbol{s}_{\boldsymbol{V},\tau}$ by $\hat{\boldsymbol{s}}_{\boldsymbol{V},\tau}$ in (19), and letting $f_k = k/(m_1\Delta_{\mathrm{t}})$, (22) becomes

$$\begin{aligned}\boldsymbol{\lambda}_k &= \sum_{\tau=0}^{\lfloor m_1/2\rfloor}\hat{\boldsymbol{s}}^T_{\boldsymbol{V},\tau}\mathrm{e}^{-\mathrm{i}2\pi f_k\tau\Delta_{\mathrm{t}}} + \sum_{\tau=\lfloor m_1/2\rfloor+1}^{m_1-1}\hat{\boldsymbol{s}}_{\boldsymbol{V},m_1-\tau}\mathrm{e}^{-\mathrm{i}2\pi f_k\tau\Delta_{\mathrm{t}}}\\ &= \sum_{\tau=0}^{\lfloor m_1/2\rfloor}\hat{\boldsymbol{s}}_{\boldsymbol{V},-\tau}\mathrm{e}^{-\mathrm{i}2\pi f_k\tau\Delta_{\mathrm{t}}} + \sum_{\tau=1}^{\lfloor m_1/2\rfloor-\delta}\hat{\boldsymbol{s}}_{\boldsymbol{V},\tau}\mathrm{e}^{-\mathrm{i}2\pi f_k(m_1-\tau)\Delta_{\mathrm{t}}}\end{aligned}$$

where $\lfloor\cdot\rfloor$ denotes integer part, $\delta = 1$ if m_1 is even, and 0 if m_1 is odd. So,

$$\begin{aligned}\boldsymbol{\lambda}_k &= \sum_{\tau=0}^{\lfloor m_1/2\rfloor} \hat{\boldsymbol{s}}_{\boldsymbol{V},-\tau} \mathrm{e}^{-\mathrm{i}2\pi f_k \tau \Delta_\mathrm{t}} + \sum_{\tau=1}^{\lfloor m_1/2\rfloor-\delta} \hat{\boldsymbol{s}}_{\boldsymbol{V},\tau} \mathrm{e}^{-\mathrm{i}2\pi f_k (-\tau) \Delta_\mathrm{t}} \\ &= \sum_{\tau=0}^{\lfloor m_1/2\rfloor} \hat{\boldsymbol{s}}_{\boldsymbol{V},-\tau} \mathrm{e}^{-\mathrm{i}2\pi f_k \tau \Delta_\mathrm{t}} + \sum_{\tau=-(\lfloor m_1/2\rfloor-\delta)}^{-1} \hat{\boldsymbol{s}}_{\boldsymbol{V},-\tau} \mathrm{e}^{-\mathrm{i}2\pi f_k \tau \Delta_\mathrm{t}} \\ &= \sum_{\tau=-(\lfloor m_1/2\rfloor-\delta)}^{\lfloor m_1/2\rfloor} \hat{\boldsymbol{s}}_{\boldsymbol{V},-\tau} \mathrm{e}^{-\mathrm{i}2\pi f_k \tau \Delta_\mathrm{t}}.\end{aligned}$$

Provided we choose $m_1 > 2(N-1)$, (20), then the fact that $\hat{\boldsymbol{s}}_{\boldsymbol{V},\tau} = \mathbf{0}$, $|\tau| \geq N$, ensures that

$$\boldsymbol{\lambda}_k = \sum_{\tau=-(N-1)}^{N-1} \hat{\boldsymbol{s}}_{\boldsymbol{V},-\tau} \mathrm{e}^{-\mathrm{i}2\pi f_k \tau \Delta_\mathrm{t}}. \tag{29}$$

Transposing throughout (29) and comparing with (26) gives $\boldsymbol{\lambda}_k^T = \hat{\boldsymbol{S}}_{\boldsymbol{V}}(f_k)/\Delta_\mathrm{t}$. Since $\hat{\boldsymbol{S}}_{\boldsymbol{V}}(f_k)$ is NND, and the transpose of a NND matrix is NND, we see that $\boldsymbol{\lambda}_k$ is NND. So the circulant embedding method can always be used to generate time series using suitable nonparametric spectral estimates of the given time series. Given a portion of length N of a vector-valued time series $\{\boldsymbol{V}_t\}$:

1. Choose an $m_1 > 2(N-1)$ a power of 2. ($m_1/2 > N-1$ so $\hat{\boldsymbol{s}}_{\boldsymbol{V},m_1/2} = \mathbf{0}$ and is therefore symmetric so that we can choose m_1 even.) Estimate the spectral matrix $\hat{\boldsymbol{S}}_{\boldsymbol{V}}(f_k)$, $f_k = k/(m_1\Delta_\mathrm{t})$, $k = 0, 1, \ldots, m_1 - 1$ (multitaper etc., [26]).

2. Set $\boldsymbol{\lambda}_k = \hat{\boldsymbol{S}}_{\boldsymbol{V}}^T(f_k)/\Delta_\mathrm{t}$, $k = 0, \ldots, m_1 - 1$.

The rest of the algorithm is as steps 3-5 of Section IV-D.

Remark 1: Asymptotically our algorithm is equivalent to that proposed in [9, sec. 4.2]. However, as explained above, our approach correctly treats the covariance structure for the practical situation of finite samples, and the use of Proposition 1 means that efficiency is doubled.

VI. Confidence Intervals by Bootstrapping

Given data samples $\{\boldsymbol{V}_t,\, t = 0, \ldots, N-1\}$ for the ocean current data we firstly compute $\hat{\boldsymbol{S}}_{\boldsymbol{V}}(f)$ using a multitaper spectral estimate with $K = 12$ sine tapers. The half-bandwidth of the induced spectral window is $W_N = (K+1)/[2(N+1)\Delta_\mathrm{t}]$ and with $N = 1600$ and $\Delta_\mathrm{t} = 1\mathrm{h}$ we get $W_N = 0.004\mathrm{c/h}$. We are interested in the low frequencies around the inertial frequency and in view of (16) and (17) we do not consider the lowest frequencies in the range $[0, W_N] = [0, 0.004]\mathrm{c/h}$.

$\hat{\boldsymbol{S}}_{\boldsymbol{U}}(f)$ can be found from (28). The statistic of interest $\hat{\theta}$, say, can be calculated from $\hat{\boldsymbol{S}}_{\boldsymbol{U}}(f)$ or $\hat{\boldsymbol{S}}_{\boldsymbol{V}}(f)$ as detailed in Section 3(b). Then using the algorithm in Section 5(b) we generate a new sample $\{\boldsymbol{V}_t^\star, t = 0, \ldots, N-1\}$ and hence $\hat{\boldsymbol{S}}_{\boldsymbol{V}}^\star(f)$ (and $\hat{\boldsymbol{S}}_{\boldsymbol{U}}^\star(f)$ if desired) and the parameter θ estimated as $\hat{\theta}^\star$. This is repeated b times to get 'parametric bootstrap' parameter estimates $\hat{\theta}_1^\star(f), \ldots, \hat{\theta}_b^\star(f)$.

The question of finding confidence intervals for θ based on $\hat{\theta}_1^\star, \ldots, \hat{\theta}_b^\star$ is discussed in [8, Chapter 5]. We considered the normal approximation, basic bootstrap, studentized bootstrap and basic percentile methods ([8, eqns. (5.5)-(5.7) and (5.18)]; using a known second-order vector autoregressive process we carried out extensive frequency domain tests and found the percentile method to be generally satisfactory. This is not unexpected given the enduring popularity of the percentile method [4, p. 1152] for which the $100(1-2\alpha)\%$ confidence interval for θ is $[\hat{\theta}^\star_{((b+1)\alpha)}, \hat{\theta}^\star_{((b+1)(1-\alpha))}]$ where $\hat{\theta}^\star_{((b+1)\alpha)}$ is the $(b+1)\alpha$th ordered value of the $\hat{\theta}^\star$; this may require rounding.

VII. Results

A. Rotary Coefficient

For the rotary coefficient we look at individual time series. From the data samples $\{\boldsymbol{V}_t = [X_t, Y_t]^T, t = 0, \ldots, N-1\}$ for any series we firstly computed $\hat{\boldsymbol{S}}_{\boldsymbol{V}}(f)$. $\hat{\boldsymbol{S}}_{\boldsymbol{U}}(f)$ follows from (28) and $\hat{S}_Z(f)$ is the top-left and $\hat{S}_Z(-f)$ the bottom-right entry in $\hat{\boldsymbol{S}}_{\boldsymbol{U}}(f)$, giving the rotary coefficient estimate

$$\hat{\rho}(f) = [\hat{S}_Z(f) - \hat{S}_Z(-f)]/[\hat{S}_Z(f) + \hat{S}_Z(-f)].$$

We generated a new sample $\{\boldsymbol{V}_t^\star, t = 0, \ldots, N-1\}$ and calculated $\hat{S}_Z^\star(f)$ and $\hat{S}_Z^\star(-f)$ and hence $\hat{\rho}^\star(f)$. This was repeated b times to get 'bootstrap' rotary coefficient estimates $\hat{\rho}_1^\star(f), \ldots, \hat{\rho}_b^\star(f)$. 95% confidence intervals were obtained by the percentile method. For $b = 10\,000$ the results are shown in Fig. 2 for frequencies $f = 0.0518, 0.0600, 0.0697, 0.1095$. At each depth and frequency the lower thick horizontal bar gives the bootstrap simulated confidence interval, while the upper thin horizontal bar denotes the theoretical confidence interval based on the estimated rotary coefficient (shown by the solid dot) from the original series There is generally good agreement between the theoretical and simulated intervals.

B. Outer Coherence

We now consider the outer coherence. From the matrix $\hat{\boldsymbol{S}}_{\boldsymbol{U}}(f)$ we firstly computed the sample estimate $\hat{\gamma}^2_{lm*}(f)$ using (11) to look for high outer coherencies. For $l = 3, m = 4$ we selected four frequencies $f = 0.0304, 0.040, 0.0415, 0.0437$(c/hr) where the estimated outer coherencies exceeded 0.4, elsewhere they are lower.

From the time series $[X_{3,t}, X_{4,t}, Y_{3,t}, Y_{4,t}]^T$, $t = 0, \ldots, N-1$, we generated $b = 10000$ bootstrap samples, and from these the 4×4 matrices $\hat{\boldsymbol{S}}^{\star}_{\boldsymbol{U},1}(f), \ldots, \hat{\boldsymbol{S}}^{\star}_{\boldsymbol{U},b}(f)$ and hence $\hat{\gamma}^{2\star}_{34*,1}(f), \ldots, \hat{\gamma}^{2\star}_{34*,b}(f)$. 95% confidence intervals were obtained by the percentile method. The results are shown in Fig. 3(a). At each of the four frequencies the right thick vertical bar gives the bootstrap simulated confidence interval, while the thin vertical bar denotes the theoretical confidence interval based on the estimated outer coherence (shown by the solid dot) from the original series 3 and 4. There is good agreement between the simulated and theoretical intervals. We notice that for $f = 0.0304$ the confidence intervals include very low coherencies, close to zero, whereas for the frequencies around 0.04 coherence always appears substantially non-zero.

Results for other pairs of series showing some notable coherence were very similar.

C. Mean Orientation

Let us turn now to the mean orientation. The theoretical distribution of its estimator depends on the nuisance parameter $\gamma^2_*(f)$ which needs to be well-estimated, the larger the better. For both series 2 and series 5 we found frequencies for which $\hat{\gamma}^2_*(f) > 0.5$: in fact, $f = 0.039, 0.041, 0.043, 0.045$ (c/h) for series 2 and $f = 0.04, 0.043, 0.055$ (c/h) for series 5.

We proceeded as for the rotary coefficient but from $\hat{\boldsymbol{S}}_{\boldsymbol{U}}(f)$, we extracted the mean orientation estimator $\hat{\theta}(f) = \arg\{\hat{R}_Z(f)\}/2$. Then we generated a new sample $\{\boldsymbol{V}^{\star}_t, t = 0, \ldots, N-1\}$ and calculated $\hat{\theta}^{\star}(f) = \arg\{\hat{R}^{\star}_Z(f)\}/2$. This was repeated $b = 10\,000$ times to get 'bootstrap' mean orientation estimates $\hat{\theta}^{\star}_1(f), \ldots, \hat{\theta}^{\star}_b(f)$ from which the 95% bootstrap confidence interval was obtained. Results are shown in Figs. 3(b) and (c) for series 2 and 5, respectively, using the same style of plot as for Fig. 3(a). Agreement between the simulated and theoretical intervals is again good, especially given the computational difficulty (Appendix-A) of finding the theoretical intervals for this angular random variable.

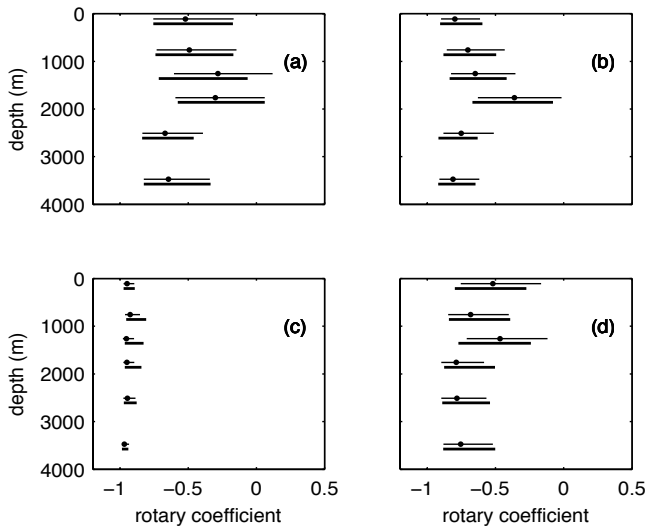

Fig. 2. Estimated rotary coefficient (solid dot), corresponding 95% theoretical confidence intervals (thin horizontal bars), and simulated confidence intervals (thick horizontal bars) for the six observation depths at frequencies (c/h) of approximately (a) 0.05, (b) 0.06, (c) 0.07, and (d) 0.11. 10000 bootstrap relications and 12 tapers were used.

VIII. Concluding Comments

While it is useful to be able to simulate real or complex vector-valued time series with exactly known ACVS — as in Section IV — it is often more useful in practice to be able to generate approximate statistical replicas using a single observed vector-valued sequence. The latter, the main topic of this paper, can be used, for example, to derive confidence intervals (i) for a parameter having an estimator whose distribution is not known analytically, or (ii) to compare with theoretical confidence intervals computed using plug-in values of nuisance parameters.

An NND estimator $\hat{\boldsymbol{S}}_{\boldsymbol{V}}(f_k)$ derived from the sample data corresponds to an NND $\boldsymbol{\lambda}_k$ so the circulant embedding algorithm can always be used to generate time series using suitable nonparametric spectral estimates of the given time series. Our circulant embedding approach correctly treats the covariance structure for the practical situation of finite samples. Two important restrictions should be highlighted. Firstly, our simulation algorithm is appropriate for Gaussian sample paths. Since the Fourier coefficients are asymptotically Gaussian under very general assumptions, this problem is pervasive in a frequency domain method. If the given sample violates the assumption of Gaussianity in the sense that a notable departure from Gaussianity is observed in the multivariate Q-Q plots, samples produced from our algorithm can be thought of as

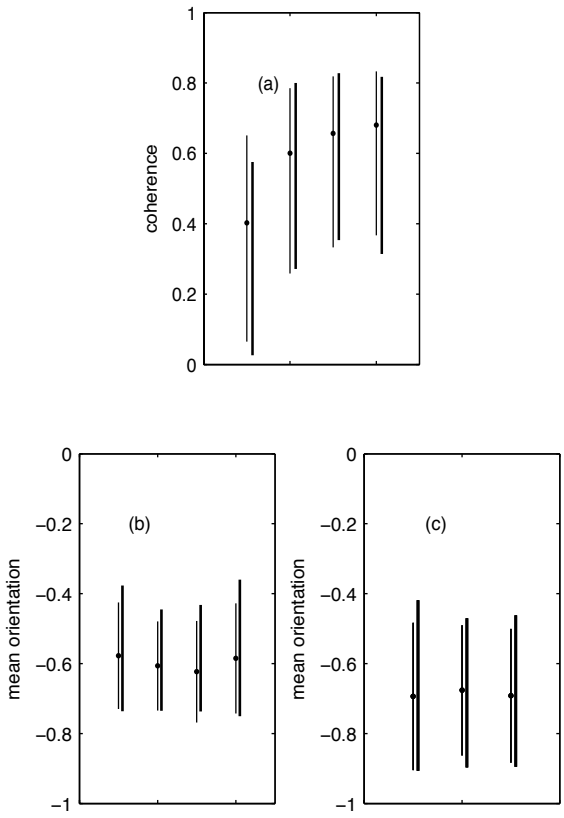

Fig. 3. (a) 95% confidence intervals for outer coherence (from series 3 and 4) at four frequencies given in the text (left to right). (b) 95% confidence intervals for mean orientation in radians for series 2 at four frequencies given in text (left to right). (c) 95% confidence intervals for mean orientation for series 5 at three frequencies given in text (left to right). In all plots the thin vertical bar denotes the theoretical confidence interval based on the estimated parameter (solid dot) and the thick bar gives the bootstrap simulated confidence interval. 10000 bootstrap relications and 12 tapers were used.

samples from a Gaussian approximation to the data generating process of the given time series. Secondly, the SDF estimators used have an ACVS that is finitely supported and the SDF estimates are continuous at zero. The methodology is not suitable for processes with long-memory since a long-memory process has an ACVS which decays very slowly towards zero, and has a discontinuity at zero frequency.

Appendix

A. Confidence Intervals for Mean Orientation

For the mean orientation estimator $\hat{\theta}(f) = \frac{1}{2}\arg\{\hat{R}_Z(f)\}$, $\hat{R}_Z(f)$ comes from the K-degrees-of-freedom estimator in (13). Let $\hat{\phi}(f) = \arg\{\hat{R}_Z(f)\}$ and $\phi(f) = \arg\{R_Z(f)\}$. Under the stationary and Gaussian assumption the PDF for $\hat{\phi}(f)$ is given by [15, eqn. (18)] (with f temporarily suppressed)

$$\begin{aligned} g(\hat{\phi};\phi,\gamma_*^2) &= \frac{\Gamma(K+\frac{1}{2})[1-\gamma_*^2]^K\beta}{2\sqrt{\pi}\Gamma(K)[1-\beta^2]^{K+\frac{1}{2}}} \\ &+ \frac{[1-\gamma_*^2]^K}{2\pi}{}_2F_1\left(K,1;\tfrac{1}{2};\beta^2\right), \end{aligned} \tag{30}$$

where $\beta = |\gamma_*|\cos([\hat{\phi}-\phi])$, $-\pi \le \hat{\phi} < \pi$, and $\gamma_*^2 < 1$. Here ${}_2F_1(\alpha_1,\alpha_2;\alpha_3;z)$ is the hypergeometric function with 2 and 1 parameters, α_1, α_2 and α_3, and scalar argument z. Now $g(\hat{\phi};\phi,\gamma_*^2)$ defines the *circular* distribution of a random variable over $[-\pi,\pi)$. The mean is given by the value ϕ_0 satisfying $E\{\sin(\hat{\phi}-\phi_0)\} = 0$, [12]. Proceeding as in [23, Section IV-B] it follows readily that $E\{\hat{\phi}\} = \phi$. To find theoretical quantiles for $\hat{\phi}$ we note that with $\tilde{\phi}$ denoting the median of $\hat{\phi}$ the $\varrho-$quantile $\tilde{\phi}_\varrho$ of its distribution is defined by

$$\int_{\tilde{\phi}-\pi}^{\tilde{\phi}_\varrho} g(\hat{\phi};\phi,\gamma_*^2)\,\mathrm{d}\hat{\phi} = \varrho, \quad 0 \le \varrho < 1, \tag{31}$$

(see [12, eqn. (3.18)], with the obvious misprint corrected). In other words we first rotate round the circle to be centred in the median direction, then integrate from π less than this up to as much as π more than this, depending on ϱ. Given an outcome $\hat{\phi}_0$ to compute a $100(1-2\alpha)\%$ confidence for ϕ we want (ϕ_1,ϕ_2) where

$$P[\hat{\phi}(\phi_1,\gamma_*^2) \ge \hat{\phi}_0] = \alpha = P[\hat{\phi}(\phi_2,\gamma_*^2) \le \hat{\phi}_0]. \tag{32}$$

If $\phi = \phi_1$ then $E\{\hat{\phi}\} = \phi_1$ and if $\phi = \phi_2$ then $E\{\hat{\phi}\} = \phi_2$, so to make the solution of (32) computationally tractable we replaced the median in the lower limit of (31) by the mean so that we find the values of ϕ_1, ϕ_2 satisfying

$$\int_{\phi_1-\pi}^{\hat{\phi}_0} g(\hat{\phi};\phi_1,\bar{\gamma}_*^2)\,\mathrm{d}\hat{\phi} = 1-\alpha; \ \int_{\phi_2-\pi}^{\hat{\phi}_0} g(\hat{\phi};\phi_2,\bar{\gamma}_*^2)\,\mathrm{d}\hat{\phi} = \alpha.$$

Unless the PDF is heavy-tailed at its extremities near $\tilde{\phi} \pm \pi$ this replacement of the median by the mean should not matter. Note again the use of the plug-in estimated and debiased coherence

$\bar{\gamma}_*^2$. Let us now restore f. Having thus found $(\phi_1(f), \phi_2(f))$, a $100(1-2\alpha)\%$ confidence interval for $\theta(f)$ is given by $(\phi_1(f)/2, \phi_2(f)/2)$.

B. Bivariate Q-Q Plots

For scalar Q-Q plots we would like to compare a set of normalized sample observations $x_1, \ldots, x_N$ (with sample mean and standard deviation of zero and one, respectively), with distribution function F_1 against a standard Gaussian reference distribution $\mathcal{N}(0,1)$ with distribution function F_2. The qth quantile of the distribution function F_2 is η_q such that $F_2(\eta_q) = q$. For $i = 1, \ldots, N$ we take the rank of x_i, say $r(x_i) = j$, and find the $q_i = j/(N+1)$ (typically) quantile of the standard Gaussian distribution $Q(q_i) = \eta_{q_i}$, where $Q \equiv F_2^{-1}$. The quantiles for F_2 are the $\{\eta_{q_i}\}$ and the quantiles for F_1 are the observations $\{x_i\}$; the Q-Q plot is $\{(x_i, \eta_{q_i}),\ i = 1, \ldots, N\}$. Points clustering about a 45° line indicate Gaussianity.

In the bivariate case we want to compare N sample bivariate observations against a spherical bivariate Gaussian distribution $\mathcal{N}_2(\mathbf{0}, \boldsymbol{I})$. The first step is to centre and sphere (normalize) the data, $\{\boldsymbol{V}_i \equiv [X_i, Y_i]^T, i = 1, \ldots, N\}$, by subtracting the sample mean and multiplying by the inverse of the sample covariance matrix to obtain $\{\check{\boldsymbol{V}}_i, i = 1, \ldots, N\}$, say. Then we find the spatial ranks

$$\boldsymbol{r}(\check{\boldsymbol{V}}_i) = \frac{1}{N} \sum_{j=1:N; \check{\boldsymbol{V}}_i \neq \check{\boldsymbol{V}}_j} \frac{\check{\boldsymbol{V}}_i - \check{\boldsymbol{V}}_j}{||\check{\boldsymbol{V}}_i - \check{\boldsymbol{V}}_j||} \in \mathbb{R}^2, i = 1, \ldots, N,$$

and then calculate the $\boldsymbol{q}_i = \boldsymbol{r}(\check{\boldsymbol{V}}_i)$ [18] spatial quantile of $\mathcal{N}_2(\mathbf{0}, \boldsymbol{I})$. (Note the division by N is included in the definition of the spatial rank.) The spatial quantile $\boldsymbol{\eta}_{\boldsymbol{q}_i}$ of the spherical bivariate Gaussian may be found as [18, Appendix A.2]

$$\boldsymbol{\eta}_{\boldsymbol{q}_i} = \boldsymbol{Q}(\boldsymbol{q}_i) \equiv (\boldsymbol{q}_i/||\boldsymbol{q}_i||) f^{-1}(||\boldsymbol{q}_i||) \in \mathbb{R}^2, \tag{33}$$

where $f(\delta) = (\delta/[2\sqrt{2}])\mathrm{e}^{-\delta^2/2}\pi^{1/2}{}_1F_1(3/2; 2; \delta^2/2)$, and ${}_1F_1(a; b; z)$ is the confluent hypergeometric function (Kummer's function), ${}_1F_1(a; b; z) = \sum_{n=0}^{\infty} \frac{a^{(n)} z^n}{b^{(n)} n!}$ with $a^{(n)} = a(a+1)\ldots(a+n-1)$. To calculate $f^{-1}(||\boldsymbol{q}_i||)$ in (33) we set $h(y) = f(y) - ||\boldsymbol{q}_i||$, so the solution to $h(y) = \mathbf{0}$, say $\tilde{y}$, is such that $f(\tilde{y}) = ||\boldsymbol{q}_i|| \Rightarrow \tilde{y} = f^{-1}(||\boldsymbol{q}_i||)$, and $\tilde{y}$ can be found using any software that finds the zero of a function. With $\check{\boldsymbol{V}}_i = [\check{V}_{i1}, \check{V}_{i2}]^T$ and $\boldsymbol{q}_i = [q_{i1}, q_{i2}]^T$, we can construct a pair of Q-Q plots: one from $\{(\check{V}_{i1}, q_{i1}\tilde{y}/||\boldsymbol{q}_i||),\ i = 1, \ldots, N\}$ and another from $\{(\check{V}_{i2}, q_{i2}\tilde{y}/||\boldsymbol{q}_i||),\ i = 1, \ldots, N\}$. If both such plots demonstrate a 45° straight-line scatter of points, then bivariate Gausianity is supported.

Acknowledgement

The authors are grateful to Jon Lilly for the Labrador Sea data and to the referees for their helpful comments.

References

[1] D. S. Bernstein, *Matrix Mathematics*. Princeton, NJ: Princeton University Press, 2005.

[2] D. R. Brillinger, *Time Series: Data Analysis and Theory (Expanded Edition)*. New York: McGraw-Hill Inc., 1981.

[3] P. J. Brockwell and R. A. Davis, *Time Series: Theory and Methods*. Second Edition. New York, Springer-Verlag, 1991.

[4] J. Carpenter and J. Bithell, "Bootstrap confidence intervals: when, which, what? A practical guide for medical statisticians," *Statistics in Medicine*, vol. 19, pp. 1141–1164.

[5] G. Chan and A. T. A. Wood, "Simulation of stationary Gaussian vector fields," *Statistics and Computing*, vol. 9, pp. 265–268, 1999.

[6] S. Chandna and A. T. Walden, "Statistical Properties of the Estimator of the Rotary Coefficient," *IEEE Transactions on Signal Processing*, vol. 59, pp. 1298–1303, 2011.

[7] E. A. K. Cohen and A. T. Walden, "A statistical study of temporally smoothed wavelet coherence," *IEEE Trans. Signal Process.*, vol. 58, pp. 2964–2973, 2010.

[8] A. C. Davison and D. V. Hinkley, *Bootstrap Methods and their Application*. Cambridge, UK: Cambridge University Press, 1997.

[9] M. Dai and W. Guo, "Multivariate spectral analysis using Cholesky decomposition," *Biometrika*, vol. 91, pp. 629–643, 2004.

[10] S. Elipot & R. Lumpkin, "Spectral description of oceanic near-surface variability," *Geophys. Res. Lett.* **35**, L05606. (doi:10.1029/2007GL032874), 2008.

[11] W. J. Emery and R. E. Thomson, *Data Analysis Methods in Physical Oceanography*. New York: Pergamon, 1998.

[12] N. I. Fisher, *Statistical Analysis of Circular Data*. Cambridge, UK: Cambridge University Press, 1993.

[13] J. Gonella, "A rotary-component method for analysing meteorological and oceanographic vector time series," *Deep-Sea Research*, vol. 19, pp. 833–46, 1972.

[14] N. R. Goodman, "Statistical analysis based on a certain multivariate complex Gaussian distribution (an introduction)," *Ann. Math. Statist.*, vol. 34, pp. 152–77, 1963.

[15] J-S. Lee, K. W. Hoppel, S. A. Mango, and A. R. Miller, "Intensity and phase statistics of multilook polarimetric and interferometric SAR imagery," *IEEE Trans. Geosci. Remote Sens.*, vol. 32, pp. 1017–28, 1994.

[16] J. M. Lilly, P. B. Rhines, M. Visbeck, R. Davis, J. R. Lazier, F. Schott, and D. Farmer,"Observing deep convection in the Labrador Sea during winter 1994/95," *Journal of Physical Oceanography*, vol. 29, pp. 2065–2098, 1999.

[17] J. M. Lilly, P. B. Rhines, "Coherent eddies in the Labrador Sea observed from a mooring," *Journal of Physical Oceanography*, vol. 32, pp. 585–598, 2002.

[18] J. I. Marden, "Bivariate QQ-plots and spider web plots," *Statistica Sinica*, vol. 8, pp. 813–826, 1998.

[19] C. N. K. Mooers, "A technique for the cross spectrum analysis of pairs of complex-valued time series, with emphasis on properties of polarized components and rotational invariants," *Deep-Sea Research*, vol. 20, pp. 1129–1141, 1973.

[20] D. B. Percival and W. L. B. Constantine, "Exact simulation of Gaussian time series from nonparametric spectral estimates with application to bootstrapping," *Statistics and Computing*, vol. 16, pp. 25–35, 2006.

[21] D. B. Percival and A. T. Walden, *Spectral Analysis for Physical Applications*. Cambridge, UK: Cambridge University Press, 1993.

[22] B. Picinbono and P. Bondon, "Second-order statistics of complex signals," *IEEE Transactions on Signal Processing*, vol. 45, pp. 411–420, 1997.

[23] P. Rubin-Delanchy and A. T. Walden, "Kinematics of complex-valued time series," *IEEE Transactions on Signal Processing*, vol. 56, 4189–4198, 2008.

[24] P. J. Schreier and L. L. Scharf, *Statistical signal processing of complex-valued data*. Cambridge, UK: Cambridge University Press, 2010.

[25] J. Theiler, S. Eubank, A. Longtin, B. Galdrikian and J. D. Farmer, "Testing for nonlinearity in time series: the method of surrogate data," *Physica D*, vol. 58, pp. 77–94.

[26] A. T. Walden, "A unified view of multitaper multivariate spectral esimtation," *Biometrika*, vol. 87, pp. 767–787, 2000.

[27] A. T. Walden, "Rotary components, random ellipses and polarization: a statistical perspective," *Phil. Trans. R. Soc. A*, vol. 371:20110554, 2013.

[28] A. T. Walden, E. J. McCoy and D. B. Percival, "The effective bandwidth of a multitaper spectral estimator," *Biometrika*, vol. 82, 201–214, 1995.

[29] S. Y. Wang and M. X. Tang, "Exact confidence interval for magnitude-squared coherence estimates," *IEEE Signal Processing Letters,* vol. 11, pp. 326–9, 2004.

[30] A. M. Yaglom, *An introduction to the theory of stationary random functions*. Dover Publications, New York, 1962.

Swati Chandna completed her B.A. in Mathematics from the University of Delhi, India in 2006. She received an M.S. degree in Mathematics from the University of Houston, Texas, U.S.A. before starting her Ph.D. studies at Imperial College London in 2009. Her research interests include frequency domain analysis of multichannel complex-valued time series and its applications in signal processing.

Andrew T. Walden (A'86-M'07-SM'11) received the B.Sc. degree in mathematics from the University of Wales, Bangor, U.K., in 1977, and the M.Sc. and Ph.D. degrees in statistics from the University of Southampton, Southampton, U.K., in 1979 and 1982, respectively. He was a Research Scientist at BP, London, U.K., from 1981 to 1990, and then joined the Department of Mathematics at Imperial College London, London, U.K., where he is currently a Professor of statistics.